Fuel 108 (2013) 824–832

Contents lists available at SciVerse ScienceDirect

Fuel

journal homepage: www.elsevier.com/locate/fuel

The spherically symmetric droplet burning characteristics of Jet-A and biofuels derived from camelina and tallow

Yu Cheng Liu *, Anthony J. Savas, C. Thomas Avedisian

Sibley School of Mechanical and Aerospace Engineering, Cornell University, Ithaca, NY 14853, United States

HIGHLIGHTS

- Camelina and tallow HRJ fuels are compared with Jet-A using spherical droplet flame.
- Jet-A is more sooty than the biofuels due to its higher aromatic content.
- Droplet burning rates of camelina and tallow HRJ fuel are very similar to Jet-A.
- The two HRJ fuels also match Jet-A in terms of flame and sooting dynamics.
- The spherically symmetric droplet flame is useful to benchmark new generation fuels.

ARTICLE INFO

Article history:
Received 2 January 2013
Received in revised form 8 February 2013
Accepted 10 February 2013
Available online 1 March 2013

Keywords:
Alternative jet fuel
Hydroprocessed biofuel
Spherically symmetric
Droplet combustion
Camelina

ABSTRACT

This study compares liquid fuel combustion characteristics of biofuels derived from camelina (POSF6152) and tallow (POSF6308) with a US domestic aviation fuel (Jet-A, POSF4658) using the spherically symmetric (one-dimensional) droplet flame configuration as the basis of comparison. A blend of camelina biofuel and Jet-A is also examined. The initial droplet diameters were fixed at 0.57 ± 0.03 mm. The biofuels studied have been considered as replacement fuels for conventional jet fuels.

Results show that the evolutions of droplet, flame, and soot shell diameters for Jet-A and the bio-fuels are very similar regardless of intrinsic compositional differences among the individual fuels. Sooting behaviors were noted to be different with Jet-A forming significantly thicker soot clouds, most likely due to its higher aromatic content compared to biofuels. The broad similarities shown in this study were consistent with results reported in the literature for performance of the same fuel systems in actual turbine and flight tests where the fuel blends examined were noted to yield essentially indistinguishable differences in overall performance. The results suggest value to the spherical droplet flame configuration to assess performance of real fuels burning under far more complex transport conditions.

1. Introduction

A dominant source of energy for transportation systems comes from liquid fuels, and their continued use in power and propulsion devices appears to be assured for the foreseeable future [1–3]. This sustained demand enhances the reliance on imports and challenges national and energy security. Liquid aviation fuels, in particular for aerospace propulsion, are responsible for 8% of the fossil fuels used in the US [4]. A strategy to reduce consumption of petroleum fuels is to blend them with alternatives that have similar physical and chemical properties and which are derived from non-food feedstocks. This approach has been reported for biofuel blends with diesel [5] and aviation fuels [6] in engine and aircraft flight test performance studies.

Bio-based synthetic paraffinic kerosene (Bio-SPK) (derived from such feedstocks as jatropha curcas, camelina, algae, and beef tallow) is a promising replacement for conventional jet fuels, with the most desired of such fuels being "drop-in" replacements [7]. To produce Bio-SPK, chemically bonded oxygen is removed from animal fats (usually consisting of triglycerides and free fatty acids) or plant oil to produce a fuel with a higher heat of combustion, and the olefins are converted to paraffins (with carbon numbers in the jet range) for better thermal stability [8]. The resulting fuel is also termed a "Hydroprocessed Renewable Jet" (HRJ) fuel or "Hydroprocessed Ester and Fatty Acids" (HEFA) fuel [9]. The potential for Bio-SPK fuels to reduce use of conventional fossil-based jet fuels is the basis for advocating that synthetic jet fuels comprise 50% of domestic aviation fuel usage by 2016 [10] for the US. Air Force and reduce 50% of carbon emissions by 2050 for global aviation [11], though HRJs apparently do not have physical properties (e.g., density, viscosity, aromatic content, etc.) that meet

* Corresponding author. Tel.: +1 6072559109.
E-mail address: yl677@cornell.edu (Y.C. Liu).

0016-2361/$ - see front matter © 2013 Elsevier Ltd. All rights reserved.
http://dx.doi.org/10.1016/j.fuel.2013.02.025

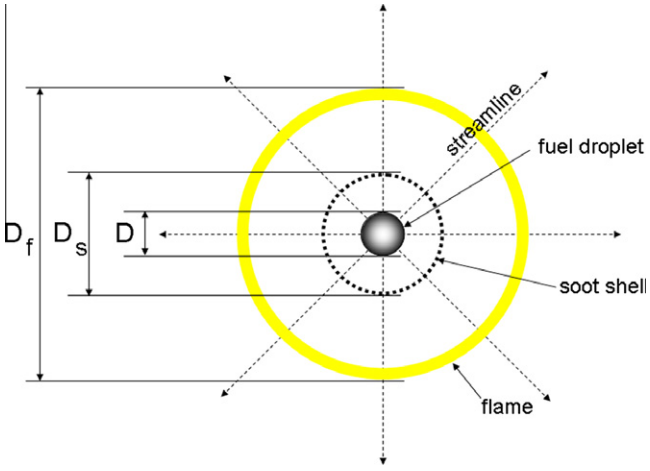

Fig. 1. Schematic of droplet burning with a spherically symmetric configuration.

certification requirements for storage, pumping, sealing, and fuel injection [12,13].

The performance of sustainable jet fuels in military and civilian aircraft has been a subject of recent interest. Assessments of the efficacy of the fuels in flight tests have often been qualitative and dependent to some extent on the specific aircraft being evaluated. For example, reports of full scale flight tests using equal-volume blends of JP8 and camelina to fuel FA/18 Super Hornet, C17 Globemaster, and A-10C Thunderbolt II aircraft indicated few differences compared to performance using neat JP8 [12,14]. On the other hand, aircraft fueled with Jet-A1 and jatropha blends showed differences in sooting and fuel efficiency in Air New Zealand, Continental Airlines and KML B747-400, and Japan Air Lines B747-300 aircraft [6,7]. The reduced aromatic content of the biofuel was thought to be responsible for the reduced soot emission. The various transport conditions experienced by fuels in different aircraft engines, or the differing blends themselves, could also be responsible for the results noted.

An important consideration for identifying a suitable combustion configuration to evaluate liquid fuels is the extent to which the configuration is amenable to detailed numerical modeling. In this way, the efficacy of the combustion chemistry, as well as tools for predicting fuel properties and radiative effects, may be assessed. A propulsion engine is too difficult to model by direct numerical simulation when considering variable properties, turbulent transport, unsteadiness, sooting, and multistep combustion chemistry effects [15]. Models can only capture processes at the sub-grid scale of simulations (e.g., droplet evaporation). Their development is based on experimental configurations that are modelable.

One or zero dimensional fluid/thermal transport processes provide a controlled environment for understanding processes at scales smaller than can be resolved in simulations. For example, gaseous or pre-vaporized liquid fuels have been studied in flow reactors and rapid compression machines, counterflow flames, and jet stirred reactors [16–19], all of which are characterized by a simple transport configuration. The information obtained is of such a fundamental nature that it is often applicable to a variety of combustion environments.

It has recently been suggested [20–22] that an isolated droplet burning under conditions where there is no relative velocity between the droplet and surrounding gas, and for which the flow is created entirely by the evaporation process, can similarly provide useful information for sub-model development, in particular to further test and validate the combustion chemistry under evaporation and combustion conditions. The configuration depicted schematically in Fig. 1 is relevant to this situation.

For the idealized configuration depicted in Fig. 1, evaporation of fuel at the droplet surface occurs by heat transfer from the high temperature flame that induces a flow into a convection-free environment resulting in a spherically symmetric burning process. Any soot aggregates that form would be trapped between the droplet and flame by the forces acting on the aggregates [23]. Combustion properties for the configuration depicted in Fig. 1 include the evolution of flame, droplet diameter, and burning rate [24]. If the fuel under consideration produces soot, the proximity of the soot shell to the droplet provides another combustion characteristic. If the flame extinguishes, the droplet diameter at extinction is an important metric to identify extinction mechanisms. Moreover, the problem of soot formation during droplet combustion has not yet been fully simulated [25,26], thus placing a high reliance on experiments in the meantime to develop the understanding of combustion performance of biofuel blends that contain components which produce soot.

The spherically symmetric droplet burning configuration incorporates many processes that arise in more complex environments such as engines where moving boundary, complex chemistry, soot formation, radiative transport and variable property effects exist [24]. The ability to model some of these aspects for the configuration of Fig. 1 has recently been demonstrated [20,21].

The present study employs the spherical droplet flame configuration to illustrate the complex processes that occur during the combustion of aviation fuels and biofuels. The droplet combustion characteristics of Jet-A (POSF4658), camelina HRJ (CHRJ, POSF6152), tallow HRJ (THRJ, POSF6308) and an equal-volume blend of CHRJ with Jet-A are studied. The equal-volume blend is examined because the performance of biofuel blends at this fractional amount was examined in engine and flight tests [6,7,12,14]. The evolution of droplet, soot shell, and flame diameters are measured. These characteristics will ultimately be useful for assessing models of droplet burning [20,21].

2. Experimental method

2.1. Droplet burning history

The droplet burning history was recorded in an apparatus designed to minimize the influence of external convection in order to promote spherical droplet flames. A low gravity condition was imposed on the droplet burning environment, "small" droplets were employed, and forced convection effects were eliminated by anchoring the test droplets to very small (14 μm) diameter SiC support structures. The elimination of buoyancy and forced convection produced nearly spherical flames. The experiments were carried out in normal atmospheric pressure air with initial droplet diameters ranging between 0.5 mm and 0.6 mm. Further details are described in [22,27]. A brief outline is given below.

A low gravity condition was developed by carrying out the experiments in an instrumentation package placed in free-fall over a 7.6 m distance to provide 1.2 s of low gravity (i.e., 10^{-4} of normal earth gravity). Fig. 2a outlines the time sequences for droplet deployment, package release, spark ignition, and electrode retraction in an experiment. High resolution digital video imaging (3.9 MP per frame, 200 fps) was used to record the droplet burning history, with backlit images highlighting the droplet and soot shell boundary and flame-illuminated images (i.e. no backlighting, recorded by a color video camera at 30 fps) providing information about the flame structure. The layout of both cameras and the combustion chamber is detailed in Fig. 2b.

Effects due to very small diameter fibers on the evaporation rate and evolution of droplet flame diameter were shown to be negligible in prior work for several organic fuels [20,22,27,28]. Droplet

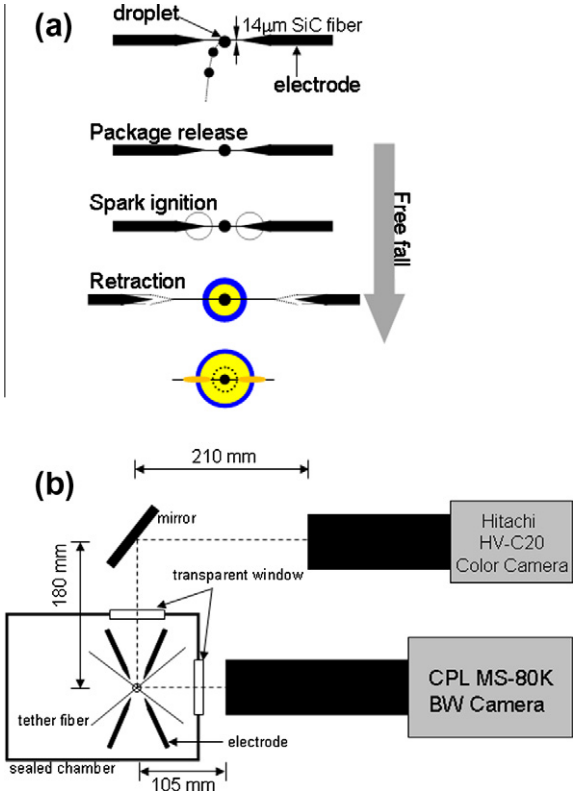

Fig. 2. Experimental procedures (a) and setup (b) in the present study.

support structures can, however, influence sooting dynamics by the aggregates being attached to the fibers as they form, and in some cases (with larger support structures) producing unusual vortex-like flow patterns [29]. Some of these effects are noted in the present study. They do not, however, detract from the efficacy of the method to provide a useful comparison of the burning characteristics of the fuels examined, which is a main objective of the present study.

2.2. Data analysis

Video imaging of the droplet burning process provides the main diagnostic from which quantitative measurements of the evolution of droplet, soot shell, and flame diameters are obtained. The droplet diameters are measured in a manual procedure using commercial software (Image-Pro v6.3). The process involves placing an ellipse area of interest (AOI) on the original image (see Fig. 3a, which is an image of a CHRJ droplet with an intact droplet boundary which is not obscured by the soot shell surrounding it) and then calculating the equivalent diameter D as $D = (H \times W)^{0.5}$ where H and W are the height and width, respectively, of the ellipse AOI. Threshold filtering [30] was not used for the images analyzed in this study because the fuels investigated produced a significant amount of soot. An example showing development of the soot shell around a burning Jet-A/CHRJ blend is shown in Fig. 3b. Progressive thickening of the shell as in Fig. 3b and c illustrates the challenge of data analysis. Here, soot almost totally obscured the droplet, thus making any sort of automated procedure for image analysis impossible to apply [30].

Soot shell diameters were measured only when there were at least three points on the outer boundary of the soot shell that could identify points on the arc of the shell. In general, the neat CHRJ and THRJ droplet burning process did not produce soot shells that totally obscured the droplets, which indicated a reduced sooting propensity for these fuels compared to Jet-A or the blends examined. The uncertainty of the measurement is estimated to be 3.4–12.6% (found by dividing two times the thickness of the gray area, ~10 pixels, by the measured droplet size, ranging from 290 to 80 pixels) for the extremes in droplet size analyzed.

We have defined the flame diameter as the outer boundary of a blue luminous zone that encloses the inner yellow (or orange) zone, depending on the fuels. Fig. 3d and e shows representative droplet flame images. The white dashed line in Fig. 3d outlines the flame boundary reported in this paper. In some cases, oxidation of soot aggregates inside the flame slightly distorted the symmetry of the inner yellow flame. This effect is ignored because it does not change the position and spherical symmetry of the outer blue zone (see Fig. 3e).

3. Fuels studied

The fuels examined consisted of biofuels, aviation fuel, and an aviation/biofuel blend: Jet-A (POSF4658) is the baseline aviation fuel against which comparisons of performance are made; CHRJ (POSF6152) and THRJ (POSF6308) were manufactured from camelina and tallow, respectively, and developed specifically for jet propulsion use; and an equal-volume mixture of Jet-A and CHRJ was examined because the equal-volume blend was previously employed in flight tests on production aircraft [6,7]. The fuels examined in the present study are all obtained from the Wright Patterson Air Force Base in Dayton, Ohio (USA). A previous study reported on the droplet burning history of Jet-A [31] which is used in the present study for comparison. Three repetitions were carried out for CHRJ and THRJ, and only one experiment is reported for the blend of Jet-A and CHRJ.

Some fuel property characteristics are shown in Table 1 and Fig. 4. CHRJ and THRJ have larger carbon numbers for their average chemical formula than does Jet-A which is consistent with our gas chromatography/mass spectrometry (GC/MS) analyses (using an Agilent 5973N GC/MS System with an electron impact detector (EID)). The lower boiling point range of the HRJ fuels compared to Jet-A as listed in Table 1 is consistent with Jet-A including heavier hydrocarbons over the whole boiling point range, while the HRJs consist mostly of iso-paraffins.

Fig. 4a shows our representative GC/MS traces for the three fuels examined while Fig. 4b indicates the fractional amount of several broad chemical classes (from [12,33]). The distribution of compounds in Jet-A is different from CHRJ and THRJ. Prominent n-paraffin peaks are indicated for Jet-A with the peaks covering a wider range of carbon number compared to CHRJ and THRJ. CHRJ and THRJ are similar to each other in terms of overall peak distributions and range of carbon numbers, except for slightly larger peaks for THRJ after a 10 min retention time. These larger peaks for THRJ are normally iso-paraffins larger than iso-C13, but they were difficult to distinguish from each other in a large pool of isomers using GC/MS analysis. Jet-A has a comparatively high aromatic content while the biofuels have virtually no aromatics (Fig. 4b). As such, we expect soot formation to be less for the biofuels compared to Jet-A, which would be manifested by thicker Jet-A soot shells compared to the biofuels. Moreover, CHRJ has 10% of cyclo-paraffins compared to 2% for tallow (see Fig. 4b) so we anticipate that CHRJ should be slightly more sooty than THRJ.

4. Results and discussions

4.1. Flame structure and sooting dynamics

Fig. 5 compares the flame structures for the HRJs examined with the Jet-A observations of Liu et al. [31]. The times are referenced to the approximate ignition point. The flames consist of the typical

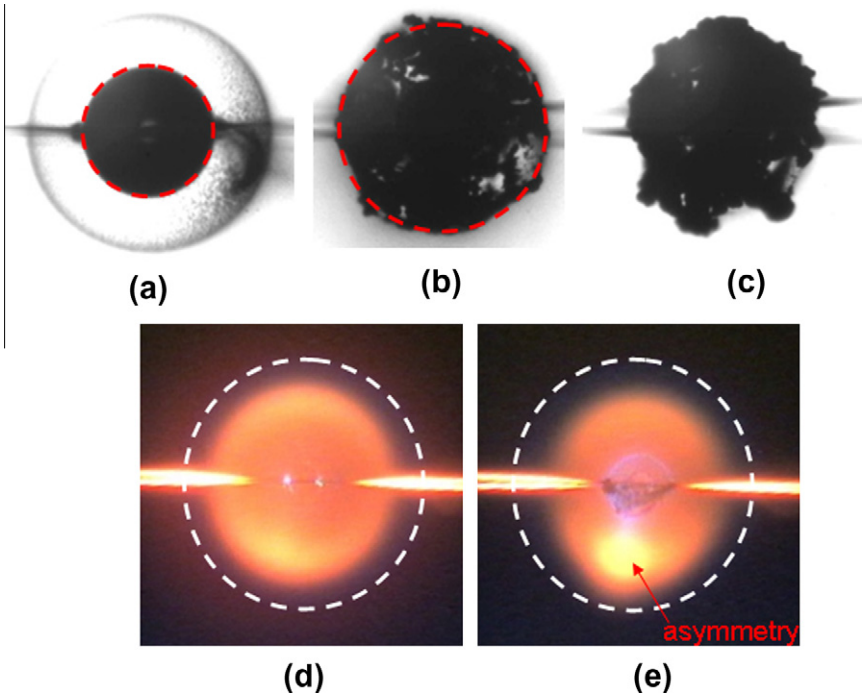

Fig. 3. Illustration of the image analysis applied to BW and color images: (a) droplet diameter measurement; (b) soot shell diameter measurement with the soot aggregate still forming a shell-like shape; (c) a BW image showing when a soot shell diameter is not measurable due to lack of a circular shape; (d) a typical color image for a flame showing that the flame diameter is defined as the outer boundary of the blue zone; (e) an image of an asymmetric yellow core as a result of irregularly shaped glowing soot aggregates. (For interpretation of the references to color in this figure legend, the reader is referred to the web version of this article.)

Table 1
Selective properties of the fuels investigated in this study.

	Jet-A (POSF4658)	CHRJ (POSF6152)	THRJ (POSF6308)
Formula	$C_{10.17}H_{19.91}$[a]	$C_{11.27}H_{24.446}$[b]	$C_{12.271}H_{26.412}$[b]
M.W. (g/mole)	142[a]	160[b]	174[b]
ρ (kg/m^3) @ 24.6 °C[c]	800	743	750
$C_{p,L}$ (kJ/kgK)[d]	1.955	2.034	1.978
k_L (W/mK)[d]	0.096	~0.108	~0.124
Boiling point (°C)	205–300[f]	151–259[g]	165–255[g]
Freeze point (°C)	<−40[f]	<−77[g]	−62[g]
Flash point (°C)	>38[f]	43[g]	55[g]
Smoke point (mm)[g]	>19	50	>40
H/C ratio	1.957[a]	2.169[b]	2.152[b]
ν[e]	15.15	17.38	18.87
ΔH_c (MJ/kg)[b]	42.8	44.3	44.1

[a] Ref. [32].
[b] Ref. [9].
[c] Measured using a digital density meter (Toledo Mettler DA-100).
[d] Ref. [13] using the value evaluated at 25 °C.
[e] Calculated from the molecular formula by assuming complete combustion.
[f] Ref. [38].
[g] Ref. [12].

inner yellow core enclosed by an outer blue zone. The yellow zone is indicative of incandescence of soot aggregates that reside between the droplet and flame. The two horizontal needle-like glows in each of the images are due to interactions between the flame and support fibers.

It is evident that Jet-A droplets have the brightest flames. This effect is consistent with the high aromatic content of Jet-A as noted previously. The HRJs do show some luminosity, though, as they contain soot-producing components (e.g., iso-paraffins). Flames for CHRJ are slightly brighter than THRJ, which is consistent with the fact that CHRJ is comprised of 10% cyclo-paraffins while THRJ has only 2%.

The sooting dynamics are clearly shown in the backlit images of Fig. 6. The soot aggregates formed during combustion are trapped at radial locations where the thermo-diffusiopheretic forces on them balance [34], which gives rise to the shell-like configuration shown in the photographs. The fiber supports somewhat influence the aggregation, coagulation, and symmetry of the soot shells (cf. Fig. 6, note the lower hemisphere of CHRJ and THRJ at 0.2 s and 0.4 s). However, the effect is not as dramatic as for droplets attached to the end of single fibers with much larger fiber diameters [29].

It is seen that Jet-A forms thicker soot clouds compared to the equal-volume blend or the neat HRJs, which is believed to be due to Jet-A's higher aromatic content as noted previously. With thick

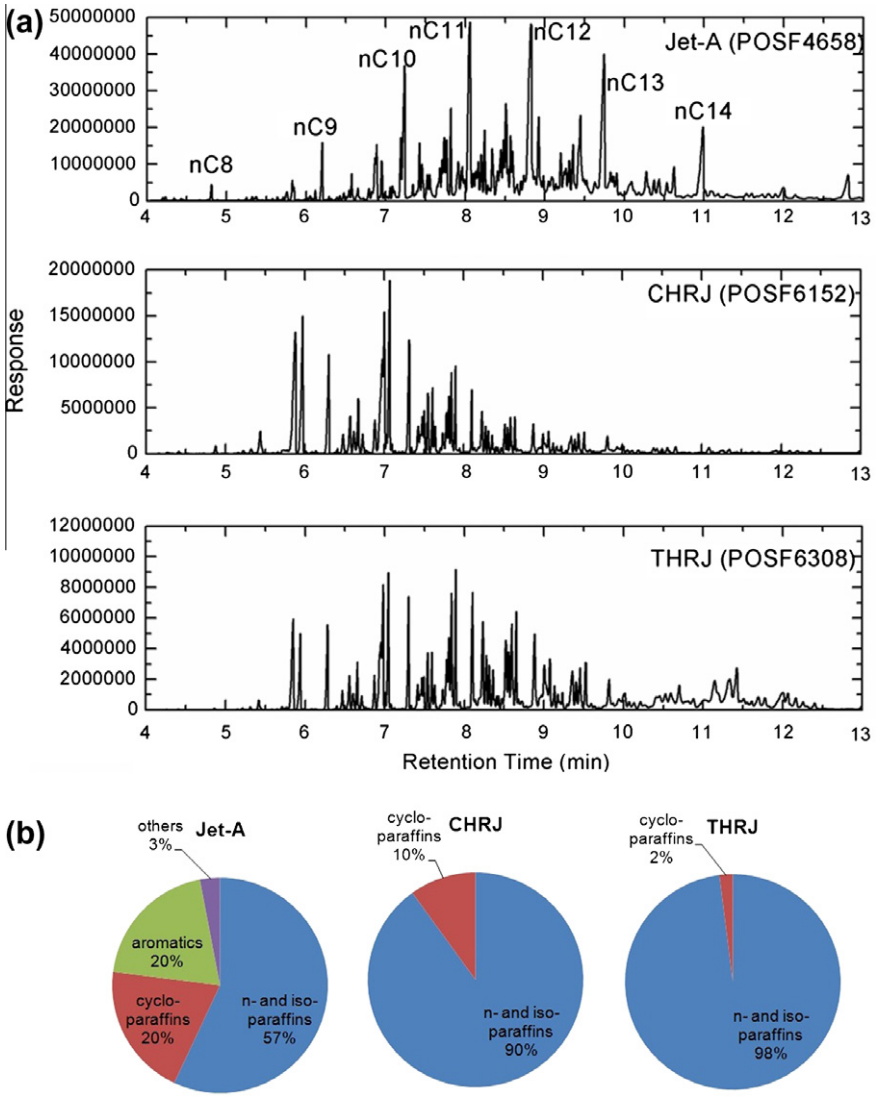

Fig. 4. (a) GC/MS peaks for Jet-A (POSF4658), CHRJ (POSF6152), and THRJ (POSF6308); (b) hydrocarbon class distribution for Jet-A [33], CHRJ, and THRJ [12] with numbers provided.

soot shells and brighter flames, a droplet can become obscured which will challenge the ability to measure the droplet diameter (D in Fig. 1). The lower sooting propensities for the HRJs shown in Fig. 6 better reveal the evolution of the soot shell that is idealized in Fig. 1. Comparisons of sooting propensities for Jet-A and HRJs are found to be qualitatively consistent with the smoke point values provided in Table 1 (higher smoke points correspond to lower sooting propensities).

4.2. Quantitative measurements

The evolution of the droplet diameter is a measure of how fast a liquid fuel is consumed (i.e., its "evaporation" or "burning" rate). The burning rate is an important parameter that characterizes performance of a fuel in a practical engine environment. For the spherically symmetric case, the burning rate is a limit parameter to which the effect of convection must revert when convection effects are eliminated. The influence of the complex swirling and turbulent motion typical of a real engine environment is completely absent under the conditions of the present study which is the base case for liquid fuel burning.

Longstanding theories of droplet burning for the simplified situation shown in Fig. 1 related the burning rate, K, to the evolution of droplet diameter, D (or more accurately stated D^2) as [24,35]:

$$\left(\frac{D}{D_o}\right)^2 = 1 - K\left(\frac{t}{D_o^2}\right) \quad (1)$$

where D is the droplet diameter (mm), t is time (s), and K is the burning rate (mm^2/s) which should theoretically be independent of D_o. Since D_o was essentially constant for the data reported here, the effect of D_o is not examined. Fig. 7 displays all of the measurements of droplet diameter in the coordinates of Eq. (1). The HRJs are very close to one another and suggest no substantive differences in burning rates between CHRJ and THRJ. The Jet-A measurements show a slightly slower burning process for some of the runs for this fuel. The lack of data (after $t/D_o^2 = 0.8$ (s/mm^2)) for the one run of the equal-volume mixture (green stars) arises because most of the droplet boundary was obscured by the surrounding thick soot shell in this particular experiment.

Fig. 8 more clearly compares the HRJs examined with Jet-A with the data averaged from Fig. 7. No significant differences in the evolution of D^2 over the first 0.8 s/mm^2 are noted. The data for CHRJ

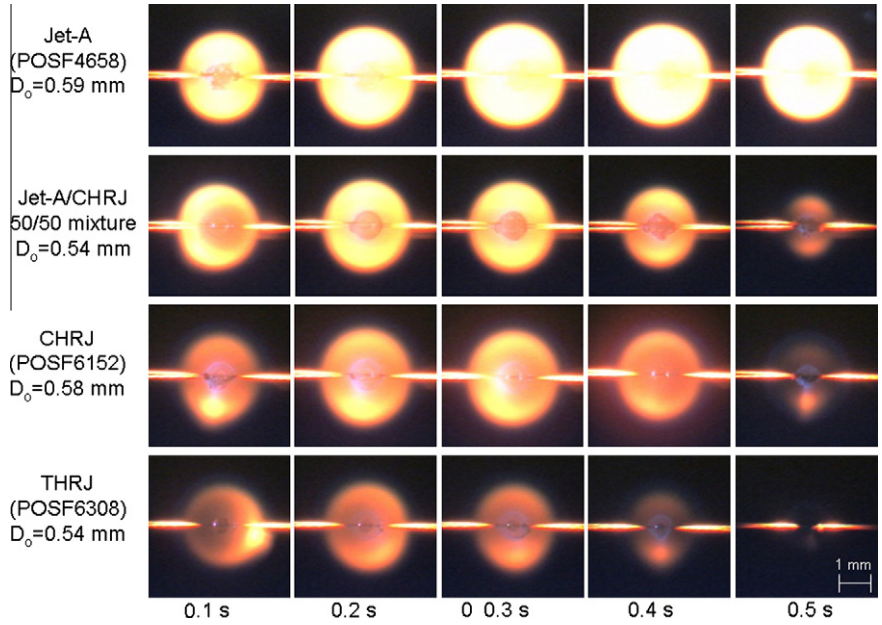

Fig. 5. Selected color images showing evolutions of outer appearances of spherical droplet flames for Jet-A (POSF4658) [31], CHRJ (POSF6152), THRJ (POSF6308), and an equal-volume blend of Jet-A and CHRJ.

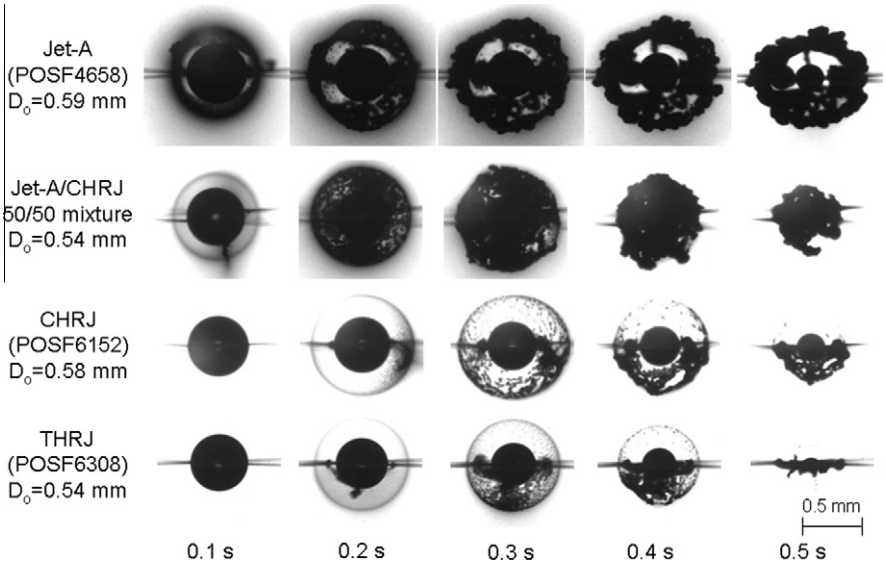

Fig. 6. Selected BW images showing evolutions of soot structures in the spherically symmetric flames of Jet-A (POSF4658) [31], the mixture of Jet-A and CHRJ, CHRJ (POSF6152), and THRJ (POSF6308).

and THRJ almost align perfectly throughout the entire combustion process. And for the Jet-A/CHRJ blend the data are almost coincident with Jet-A, indicating that adding HRJ to Jet-A does not appreciably alter the evolution of $(D/D_o)^2$. There are, however, differences in sooting dynamics as noted previously (Fig. 6). This may suggest that the formation of soot itself might not exert a strong influence on the thermal and chemical effects on which the evaporation rate depends. Further work is needed to better understand this effect.

Fig. 9 compares the burning rates among the fuels examined. The data of Fig. 8 are correlated with a fourth order polynomial fit from which the derivative is taken to obtain the burning rate (other polynomial fits to data like those shown in Fig. 8 have been considered [36]). The conformance of the burning rates over most of the burning history is evident. The burning rates initially increase during the transient droplet heating process ($t/D_o^2 < 0.8$ (s/mm^2)), then appear to reach a quasi-steady value between 0.8 s/mm^2 < t/D_o^2 < 1.2 s/mm^2 for each fuel where they are relatively constant. That the burning rates of CHRJ and THRJ are quite close is consistent with their compositions being similar (cf. Fig. 4). Interestingly, the burning rate of Jet-A is close to the HRJs during the initial droplet heating period but is noticeably lower in the quasi-steady period. Compounds in Jet-A with higher boiling points (e.g., aromatics or paraffins with large molecular weights) can lead to lower burning rates.

Fig. 10 shows evolutions of flame diameters for the fuels investigated. The measurements are scaled with the instantaneous droplet diameter to give a "flame standoff ratio", FSR = D_f/D, which is a measure of the relative position of the flame to the droplet. The classical theory of droplet burning [24,35] shows that D_f/D should

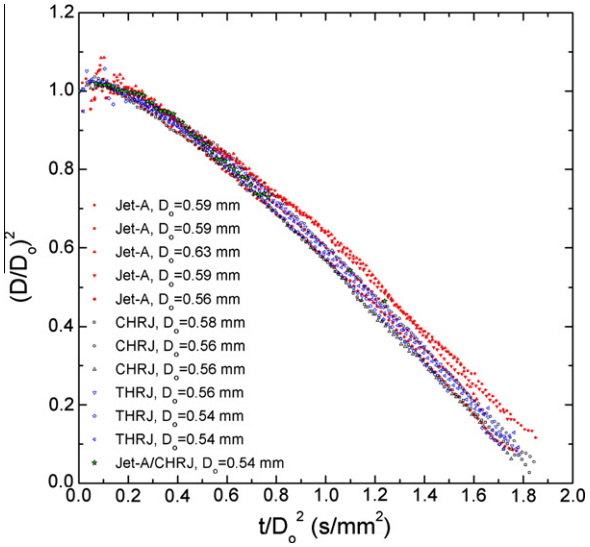

Fig. 7. Evolution of measured droplet size (D^2 plot) during combustion for the fuels investigated in this study. This plot includes data from all the individual experiments.

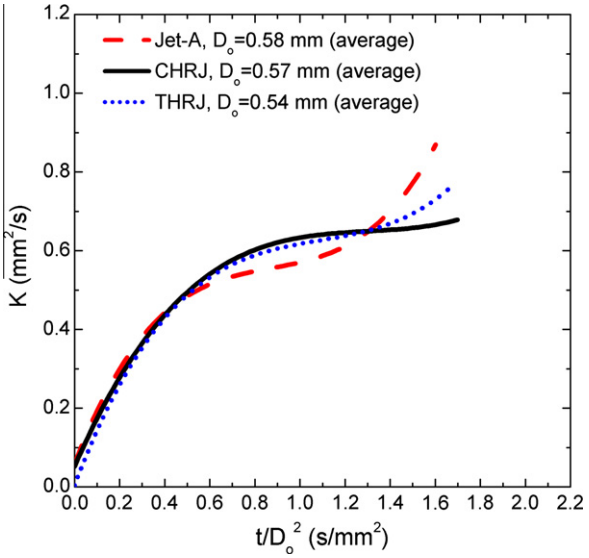

Fig. 9. Evolution of burning rate K (mm^2/s) calculated by taking the derivative of a 4th order polynomial fitted to the averaged D^2 data shown in Fig. 8.

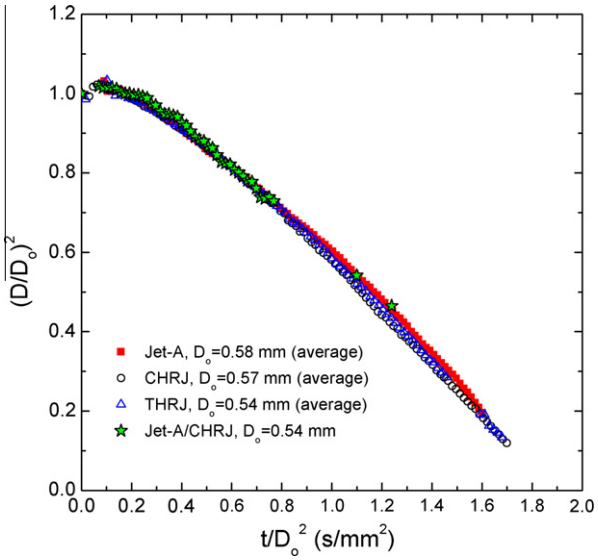

Fig. 8. Evolution of averaged D^2 data from Fig. 7 for each fuel.

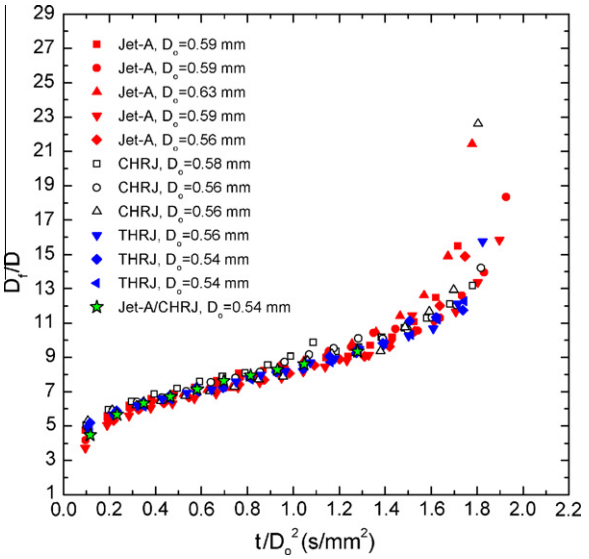

Fig. 10. Evolution of flame standoff ratio (FSR = D_f/D) for all the fuels investigated in this study.

be constant. This is clearly not the case for the data in Fig. 10, which reflects an unsteadiness in the burning process that is persistent throughout the burning history. The relative position of the flame to the droplet surface is reasonably close for Jet-A and the biofuels examined, reflecting a thermo/chemical dynamic that is consistent with the conformance of burning rates noted previously (cf. Figs. 8 and 9).

The relative position of the soot shell to the droplet surface (D_s/D), or the "soot standoff ratio" (SSR), is shown in Fig. 11. The SSR is the most difficult quantity to measure especially when the aggregates form thick soot shells (cf. Fig. 6). Given this fact, the SSR data in Fig. 11 suggest a similar relative position of the soot cloud to the droplet surface. The SSR trends are reasonably close for $t/D_o^2 < 0.9$ s/mm^2, and the SSR for the Jet-A/CHRJ blend is between that of Jet-A and CHRJ reflecting a dilution effect. Near the end of burning it is more challenging to assume a definite geometrical shape to the soot cloud because of the thickening of the cloud and coagulation of aggregates into a contiguous and self-supported structure that is less influenced by the forces acting on the aggregates. Nonetheless, the broad trends for the fuels examined are consistent with each other later in the burning process.

Fig. 12 shows a bubble inside of a THRJ droplet at 0.45 s and 0.46 s. At 0.47 s, the droplet diameter is noticeably smaller suggesting a sudden escape of the bubble from the liquid mass over a time interval shorter than 0.005 s. The droplet diameter data during bubble formation are removed from Figs. 7 and 8 since they do not represent the actual diameter of a "liquid" droplet. Since the droplets were supported by solid (albeit rather small) structures and HRJs are highly multi-component blends with components that have a range of boiling points, the potential for an internal superheating effect that could lead to bubble formation is viable. Furthermore, diffusion of volatile and condensable combustion products to the droplet surface and their subsequent dissolution in the droplet could contribute to this effect of trapping volatile species inside the droplet as the droplet heats up during combustion.

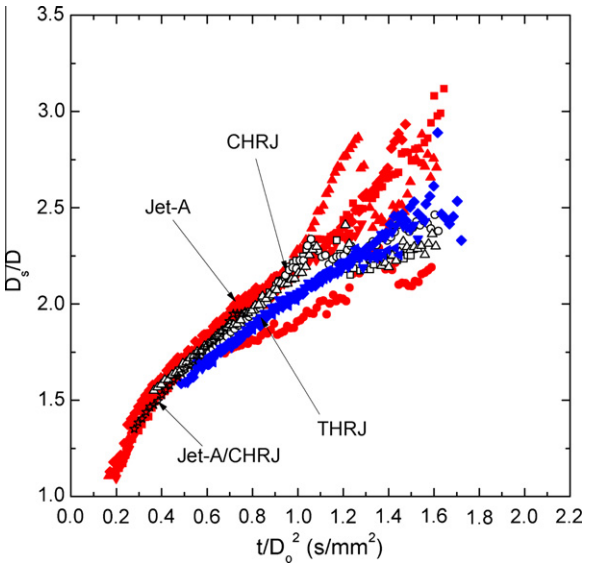

Fig. 11. Evolution of soot standoff ratio (SSR = D_s/D) for all the fuels investigated in this study. This plot includes data for all individual runs.

4.3. Effect of fuel properties on droplet burning

Even though the biofuels examined here have different chemical compositions (Fig. 4) and sooting propensities (Fig. 6), their burning rates are similar to Jet-A. Such a result is qualitatively consistent with full scale turbine tests [6] in which HRJs were subjected to a far more complex burning environment than examined here. No significant differences were found in engine performance.

From the perspective of the classic droplet combustion theory [35], the burning rate K (mm^2/s) is predominantly proportional to fuel properties as:

$$K \propto \frac{k_g}{\rho_L C_{p,g}} \tag{2}$$

where k_g is an average gas thermal conductivity, ρ_L is liquid density, and $C_{p,g}$ is an average specific heat of the combustion gas. The gas properties are not easily estimated for the fuels examined in this study due to the complexity of the compositions. The representative data in Table 1 shows small differences between the fuels. The difficulty of the classical theory is the assumption of constant properties that necessitates determining suitable average properties for prediction. If it is assumed that the gas phase properties will not vary significantly, the liquid density in Eq. (2) becomes controlling as $K \sim 1/\rho_L$. The liquid density for the Jet-A used in this study (cf. Table 1) is slightly higher than the liquid densities for the HRJs, indicating lower burning rates for Jet-A. This prediction is broadly consistent with the burning rates obtained from the experiments during the quasi-steady period ($K_{Jet\text{-}A}/K_{HRJs} \sim 0.92$ compared to $(1/\rho_{L,Jet\text{-}A})/(1/\rho_{L,HRJs}) \sim 0.93$). The lower burning rate for Jet-A in the quasi-steady period can also be attributed to its lower heat of combustion compared to the HRJs. It is also noted that the lower heat of combustion of Jet-A can be related to its higher aromatic content, and the presence of these aromatics leads to soot formation (thus a lower burning rate) which could make Jet-A a less efficient fuel than the HRJs. This observation is also consistent with flight test observations for Jet-A and the HRJs [6].

Regarding the FSR, insights into the influence of parameters is obtained from a modification of the classical theory by Aharon and Shaw [37] which shows that:

$$\Theta_{HRJ} \equiv \frac{FSR_{HRJ}}{FSR_{Jet\text{-}A}} \approx \left(\frac{\rho_{L,HRJ}}{\rho_{L,Jet\text{-}A}}\right)\left(\frac{K_{HRJ}}{K_{Jet\text{-}A}}\right)\left(\frac{\nu_{HRJ}}{\nu_{Jet\text{-}A}}\right)\left(\frac{MW_{Jet\text{-}A}}{MW_{HRJ}}\right) \tag{3}$$

where ν is the stoichiometric ratio under the assumption of complete combustion, $C_mH_n + \nu O_2 = mCO_2 + (n/2)\ H_2O$ ($\nu = m + n/4$). With the data from Table 1, Θ_{CHRJ} and Θ_{THRJ} are found to be 1.07 and 1.04, respectively, meaning that CHRJ and THRJ flames should be further from the droplet than Jet-A flames. This small difference is consistent with Fig. 10.

The results presented here show that the spherically symmetric flame configuration provides a useful quantitative comparison for the combustion performance of Jet-A and HRJs. The trends found from the experiments are surprisingly consistent with tests reported in the literature in practical engine systems and flight evaluations of these fuels.

5. Conclusions

The droplet combustion characteristics of hydroprocessed biofuels derived from camelina and tallow were studied in an environment that promotes spherical droplet flames, and the results were compared to a conventional aviation fuel, Jet-A. The results are as follows:

(a) The biofuels examined have a much lower sooting propensity than Jet-A that tracks with their lower biofuel aromatic content.
(b) Despite their sooting and fuel property differences, the biofuels and Jet-A have very similar behaviors in terms of their burning histories, burning rates, and the evolutions of the flame and soot standoff ratios.
(c) An equal-volume blend of camelina and Jet-A had sooting propensities intermediate between Jet-A and camelina biofuel showing the effect of dilution.

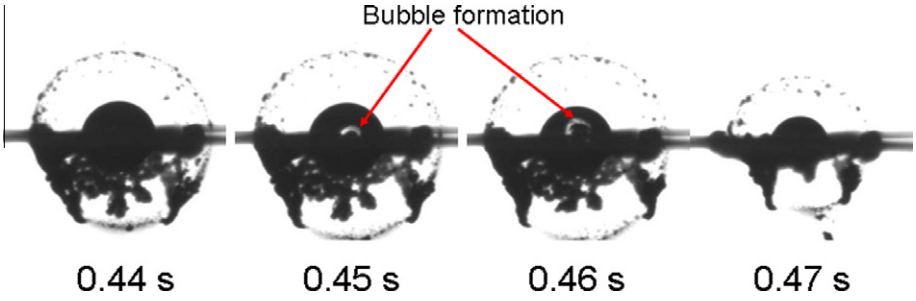

Fig. 12. Selected BW images of a THRJ droplet flame showing the effect of internal bubble formation on the soot shell and droplet. The bubble is indicated by the red arrow. The droplet at 0.47 s is noticeably smaller, most likely because of ejection of a bubble from the liquid droplet. (For interpretation of the references to color in this figure legend, the reader is referred to the web version of this article.)

(d) The results presented here that are based on the fundamental spherically symmetric droplet flame configuration are qualitatively consistent with observations from full scale flight and engine tests that showed similar performances among the fuels examined, thereby suggesting that individual droplets can provide insights into burning under complex transport conditions, with the spherically symmetric configuration being the most basic for liquid fuel combustion.

Acknowledgments

This work was supported by the National Administration of Space and Astronautics under Grant No. NNX08AI51G. The authors thank Michael Hicks of NASA for serving as the Project Monitor and for helpful discussions. The authors appreciate the generous supply of Jet-A and the HRJs used in the experiments from Tim Edwards of the Wright Patterson Air Force Base (Dayton, OH) as well as useful discussions with him.

References

[1] Transforming combustion research through cyberinfrastructure. Committee on Building Cyberinfrastructure for Combustion Research, National Research Council, The National Academies Press, ISBN-13: 978-0-309-16387-3, April, 2011. <http://www.nap.edu/catalog.php?record_id=13049>.
[2] A workshop to identify research needs and impacts in predictive simulation for internal combustion engines (PreSICE). Office of Energy Efficiency and Renewable Energy, Office of Science, U.S. Department of Energy, March 3, 2011. <http://www1.eere.energy.gov/vehiclesandfuels/pdfs/presice_rpt.pdf>.
[3] Edwards TF. Liquid fuels and propellants for aerospace propulsion: 1903–2003. AIAA J Propul Power 2003;19(6):1089–107.
[4] Transportation overview. Center for Climate and Energy Solutions. <http://www.c2es.org/technology/overview/transportation>.
[5] Patterson J, Hassan MG, Clarke A, Sharma G, Hellgardt K, Chen R. Experimental study of DI diesel engine performance using three different biodiesel fuels, SAE Paper no. 2006-01-0234.
[6] Rahmes TF, Kinder JD, Henry TM, Crenfeldt G, LeDuc GF, Zombanakis GP et al. Sustainable bio-derived synthetic paraffinic kerosene (Bio-SPK) jet fuel flights and engine tests program results. In: AIAA Paper no. 2009-7002, 9th AIAA aviation technology, integration, and operations conference (ATIO), Hilton Head, South Carolina, 21–23 September, 2009.
[7] Blakey S, Rye L, Wilson CW. Aviation gas turbine alternative fuels: a review. Proc Comb Inst 2011;33:2863–85.
[8] Kinder JD, Rahmes T. Evaluation of bio-derived synthetic paraffinic kerosene (Bio-SPK). The Boeing Company, Sustainable Biofuels Research & Technology Program; 2009. <http://www.ascension-publishing.com/BIZ/Bio-SPK.pdf>.
[9] Hui X, Kumar K, Sung C-J, Edwards T, Gardner D. Experimental studies on the combustion characteristics of alternative jet fuels. Fuel 2012;98:176–82.
[10] Blackwell KE. The Department of Defense: reducing its reliance on fossil-based aviation fuel – issues for Congress. CRS Report for Congress, Order Code RL34062; June 15, 2007.
[11] Powering the future of flight, the six easy steps to growing a viable aviation biofuels industry. Air Transport Action Group; March 2012. <http://atag.org/component/downloads/downloads/152.html>.
[12] Corporan E, Edwards T, Shafer L, DeWitt MJ, Klingshirn C, Zabarnick S, et al. Chemical, thermal stability, seal swell, and emissions studies of alternative jet fuels. Energy Fuels 2011;25:955–66.
[13] Bessee GB, Hutzler SA, Wilson GR. Propulsion and power rapid response research and development (R&D) support. Delivery order 0011: analysis of synthetic aviation fuels, Interim Report, Southwest Research Institute (SwRI), AFRL-RZ-WP-TR-2011-2084; April, 2011.
[14] IATA 2010 Report on alternative fuels, 5th ed., International Air Transport Association, Montreal-Geneva. Ref. No: 9709-03; 2010.
[15] Reitz RD. Directions in internal combustion engine research. Combust Flame 2013;160:1–8.
[16] Kumar K, Sung C-J. A comparative experimental study of the autoignition characteristics of alternative and conventional jet fuel/oxidizer mixtures. Fuel 2010;89:2853–63.
[17] Allen C, Toulson E, Edwards T, Lee T. Application of a novel charge preparation approach to testing the autoignition characteristics of JP-8 and camelina hydroprocessed renewable jet fuel in a rapid compression machine. Combust Flame 2012;159:2780–8.
[18] Mzé-Ahmed A, Hadj-Ali K, Diévart P, Dagaut P. Kinetics of oxidation of a synthetic jet fuel in a jet-stirred reactor: experimental and modeling study. Energy Fuels 2010;24:4904–11.
[19] Kick T, Kathrotia T, Braun-Unkhoff M, Riedel U. An experimental and modeling study of laminar flame speeds of alternative aviation fuels. In: Proceedings of ASME Turbo Expo., vol. 2, GT2011-45606, Vancouver, British Columbia, Canada, June 6–10, 2011. p. 579–589.
[20] Liu YC, Farouk T, Savas AJ, Dryer FL, Avedisian CT. On the spherically symmetrical combustion of methyl decanoate droplets and comparisons with detailed numerical modeling. Combust Flame 2013;160:641–55.
[21] Farouk TI, Liu YC, Savas AJ, Avedisian CT, Dryer FL. Sub-millimeter sized methyl butanoate droplet combustion: Microgravity experiments and detailed numerical modeling. Proc Combust Inst 2013;34:1609–16.
[22] Liu YC, Avedisian CT. A comparison of the spherical flame characteristics of sub-millimeter droplets of binary mixtures of n-heptane/iso-octane and n-heptane/toluene with a commercial unleaded gasoline. Combust Flame 2012;159:770–83.
[23] Avedisian CT. Recent advances in soot formation from spherical droplet flames at atmospheric pressure. J Propul Power 2000;16:628–35.
[24] Sirignano WA. Fluid dynamics and transport of droplets and sprays. Cambridge University Press; 1999. p. 10 [chapter 2].
[25] Kumar S, Ray A, Kale SR. A soot model for transient, spherically symmetric n-heptane droplet combustion. Combust Sci Technol 2002;174:67–102.
[26] Avedisian CT, Yang JC, Wang CH. On low-gravity droplet combustion. Proc R Soc London A 1988;420:183–200.
[27] Bae JH, Avedisian CT. Experimental study of the combustion dynamics of jet fuel droplets with additives in the absence of convection. Combust Flame 2004;137:148–62.
[28] Farouk T, Dryer FL. Tethered methanol droplet combustion in carbon-dioxide enriched environment under microgravity conditions. Combust Flame 2012;159:200–9.
[29] Avedisian CT, Jackson GS. Soot patterns around suspended n-heptane droplet flames in a convection-free environment. J Propul Power 2000;16:974–9.
[30] Dembia CL, Liu YC, Avedisian CT. Automated data analysis for consecutive images from droplet combustion experiments. Image Anal Stereol 2012;31:137–48.
[31] Liu YC, Savas AJ, Avedisian CT. Spherically symmetric droplet combustion of three and four component miscible mixtures as surrogates for Jet-A. Proc Combust Inst 2013;34:1569–76.
[32] Dooley S, Won SH, Chaos M, Heyne J, Ju Y, Dryer FL, et al. A jet fuel surrogate formulated by real fuel properties. Combust Flame 2010;157:2333–9.
[33] Violi A, Yan S, Eddings EG, Sarofim AF, Granata S, Faravelli T, et al. Experimental formulation and kinetic model for JP-8 surrogate mixtures. Combust Sci Technol 2002;174:399–417.
[34] Ben-Dor G, Elperin T, Krasovit B. Effect of thermo- and diffusiophoretic forces on the motion of flame-generated particles in the neighbourhood of burning droplets in microgravity conditions. Proc R Soc London A 2003;459:677–703.
[35] Turns SR. An introduction to combustion. 2nd ed. McGraw-Hill Inc.; 2006. p. 391 [chapter 10].
[36] Liu YC, Savas AJ, Avedisian CT. A comparison of the burning characteristics of indolene and commercial grade gasoline droplets without convection. Energy Fuels 2012;26:5740–9.
[37] Aharon I, Shaw BD. On the roles of thermal diffusion and distinct binary diffusion coefficients in modeling droplet flame locations in microgravity. Microgravity Sci Technol 1997;X-2:75–85.
[38] Colket M, Edwards T, Williams S, Cernansky NP, Miller DL, Egolfopoulos F et al. Development of an experimental database and kinetic models for surrogate jet fuels. In: 45th AIAA Aerospace Sciences Meeting and Exhibit, Reno, Nevada; 2007 [AIAA-2007-0770].